A simple, accurate scheme for the flow of an electric charge distribution

Sci. Rep. Kanazawa Univ. **ARTICLES**
Vol. 66, pp. 1–16, 2023

A simple, accurate scheme for the flow of an electric charge distribution

Lalita APISORNPANICH and Patrick VAN MEURS*

Faculty of Mathematics and Physics, Institute of Science and Engineering, Kanazawa University
Kanazawa, 920-1192, Japan

(Received March 7, 2023 and accepted in revised form June 2, 2023)

Abstract We consider a PDE which describes the evolution of an electric charge distribution in one spatial dimension. Due to the (singular) electrostatic interaction, the PDE is nonlocal. Moreover, the PDE describes the neutralization of charge at points where the charge distribution changes sign. Despite these complex features of the PDE, we develop a simple scheme to solve the PDE numerically. We demonstrate by means of simulations that the scheme is accurate and that it preserves the (expected) properties of the exact solution.

Keywords. Coulomb interaction, continuity equation, nonlinear diffusion, finite volume method.
2020 MSC. 65M08, 65M22, 35A21

1 Introduction

We are interested in computing numerically the evolution of an electric charge distribution κ in one spatial dimension. The flow of this charge distribution at a point x is given directly by the (nonlocal) electrostatic force induced by the charge distribution surrounding x. When two blobs of positive and negative charge meet, they gradually neutralize each other at the contact point. This neutralization is such that the net charge remains constant.

In more detail, for any $T > 0$ we consider the problem given informally by

$$\begin{cases} \dfrac{\partial \kappa}{\partial t} = -\dfrac{\partial}{\partial x}\big(|\kappa|\,(g*\kappa)\big) & 0 < t < T,\ x \in \mathbb{R} \\ \kappa(x,0) = \kappa^{\circ}(x) & x \in \mathbb{R}, \end{cases} \tag{P}$$

where $\kappa = \kappa(x,t)$ is the (signed) charge density,

$$v(x,t) := (g*\kappa(\cdot,t))(x) := \mathrm{PV}\int_{\mathbb{R}} g(x-y)\kappa(y,t)dy \tag{1.1}$$

is the flow field (with nonlocal dependence on κ),

$$g(x) := \frac{1}{x}$$

*Corresponding author Email: pjpvmeurs@staff.kanazawa-u.ac.jp.

is the electrostatic force and $\kappa^\circ \in L^p(\mathbb{R})$ for some $p > 1$ is an initial condition. Since g is not integrable at 0, the integral in (1.1) needs to be defined carefully. The principal value integral exists at least when κ is sufficiently regular. The convolution by g is known as the Hilbert transform; it can be extended as a bounded linear operator from $L^p(\mathbb{R})$ to itself for any $1 < p < \infty$.

Problem (P) can alternative be interpreted as a model for two competing species. The densities of the species' distributions are the positive and negative parts $\kappa^\pm \geq 0$ of κ (note that $\kappa = \kappa^+ - \kappa^-$). Since the interior of the supports of κ^+ and κ^- are disjoint, we obtain from (P) that $\kappa^\pm$ satisfy the continuity equations given informally by

$$\begin{cases} \dfrac{\partial \kappa^+}{\partial t} = -\dfrac{\partial}{\partial x}\big(\kappa^+ (g * (\kappa^+ - \kappa^-))\big) & 0 < t < T,\, x \in \operatorname{int}(\operatorname{supp} \kappa^+(\cdot,t)) \\ \dfrac{\partial \kappa^-}{\partial t} = -\dfrac{\partial}{\partial x}\big(\kappa^- (-g * (\kappa^+ - \kappa^-))\big) & 0 < t < T,\, x \in \operatorname{int}(\operatorname{supp} \kappa^-(\cdot,t)) \end{cases} \tag{1.2}$$

with free boundaries. Note that both equations are similar, but that κ^- evolves with the negative of the flow field v, which is natural for an electric charge density. In (P), this is encoded by the factor $|\kappa|$. Moreover, the factor $|\kappa|$ in (P) implicitly encodes the evolution of the free boundaries in (1.2): it results in the cancellation of charge density (or neutralization of charge) at *contact points*, i.e. points x where κ changes sign.

The motivation for studying problem (P) does not come from the field of electrodynamics. Instead, it appears in plasticity theory and in quasi geostrophic equations (see [BKM10, vMPP22] and references therein). [BKM10] establishes a proper solution concept for (P) and proves several properties of the solution; see Section 2 below. Here and henceforth we will adopt this solution concept, and interpret (P) in the classical sense only at points (x,t) around which κ is regular and $\kappa(x,t) \neq 0$. Building a meaningful solution concept was a challenging task due to the nonlocal, nonlinear and singular nature of the PDE. Very recently, [vMPP22] proved that (P) appears in the limit $n \to \infty$ of the particle system governed by

$$\frac{dx_i}{dt} = \frac{B}{n} \sum_{\substack{j=1 \\ j \neq i}}^{n} \frac{b_i b_j}{x_i - x_j}, \qquad i = 1, \ldots, n, \tag{1.3}$$

where n is the number of particles, $B = \int_{\mathbb{R}} |\kappa^\circ(x)| dx$ is the total charge at initial time, and $x_i = x_i(t) \in \mathbb{R}$ and $b_i \in \{-1, 1\}$ are respectively the position and charge of particle i. Upon collision, particles of opposite charge are removed from the system.

However, we are not aware of a properly motivated numerical scheme for computing solutions to (P). This motivates the aim of this paper, which is the construction of such a scheme, a numerical investigation of its accuracy, and a description of the features of the numerical solution to (P).

The paper is organized as follows. In Section 2 we list properties of the solution κ. In Section 3 we develop the scheme for solving (P) numerically. In Section 4 we investigate numerically the performance of the scheme, and use the scheme to describe features of the numerical solution to (P). Section 5 contains the conclusion.

2 Properties of the solution κ

We list several properties of problem (P) and its solution which will aid the construction of the scheme in Section 3. To the best of our knowledge, the first (and only) solution concept of (P) was found in 2008 in [IMR08, BKM10]. By integrating the equation in space, it turns out that the integrated equation satisfies a comparison principle for a suitable notion of viscosity solutions.

In particular, this implies the uniqueness of such solutions. The existence of solutions is shown for any $T > 0$ and any $\kappa^\circ \in L^1(\mathbb{R}) \cap L^p(\mathbb{R})$ where $p \in (1,\infty]$ can be chosen freely (actually, in [BKM10] a slightly more general class of initial conditions is considered, but this is not relevant for the contents of our paper). Moreover, for such κ° the solution $\kappa(\cdot,t)$ remains in $L^1(\mathbb{R}) \cap L^p(\mathbb{R})$ for all $t > 0$.

In addition, [BKM10] constructs a self-similar solution for the integrated PDE in (P), which translates to

$$\kappa_*(x,t) = \frac{1}{2\pi t}\sqrt{[4Nt - x^2]_+}, \tag{2.1}$$

where

$$N = \int_{\mathbb{R}} \kappa_*(x,t)dx$$

is a parameter (independent of t) which equals the net charge. Note that the graph of $\kappa_*(\cdot,t)$ is a half-ellipse centred at 0. By the translation invariance of the PDE, $\kappa_*(x - x_0, t + t_0)$ is also a solution for any $x_0 \in \mathbb{R}$ and any $t_0 \geq 0$. By the symmetry between positive and negative charge, also $-\kappa_*$ is a solution. Moreover, [BKM10] shows that κ_* is stable, in the sense that the solution $\kappa(\cdot,t)$ of (P) converges to $\kappa_*(\cdot,t)$ as $t \to \infty$ with parameter $N = \int_{\mathbb{R}} \kappa^\circ(x)\,dx$.

Based on these facts, we make two further predictions on the properties of the solution to (P) which we will use to test our scheme:

1. Since the self-similar solution κ_* has compact support for all $t > 0$, we expect that if κ° has compact support, then also $\kappa(\cdot,t)$ has compact support for all $t > 0$.
2. We expect that the net charge
$$N(t) := \int_{\mathbb{R}} \kappa(x,t)dx \tag{2.2}$$
is conserved.

Regarding the second prediction, we remark that the total charge given by

$$B(t) := \int_{\mathbb{R}} |\kappa(x,t)|dx \tag{2.3}$$

is, however, not expected to be conserved due to the possible cancellation of charge. Instead, we expect B to be non-increasing.

3 The scheme

First, in Section 3.1 we give a motivation for the scheme. We state the scheme precisely in Section 3.2, and in Section 3.3 we list several of its properties.

3.1 Motivation of the scheme

The scheme is based on the finite volume method with explicit Euler time integration. Motivated by the prediction in Section 2 that the support of the solution $\kappa(\cdot,t)$ is compact, we discretize (P) on a bounded interval $[a,b]$. We put zero-flux boundary conditions at a and b such that the net charge will be conserved (see Proposition 3.1 below).

Next we introduce the uniform spatial grid. Let $M \geq 1$ be the number of cells,

$$\begin{aligned} x_i &:= a + (b-a)\frac{i}{M} && (i = 0, \dots, M), \\ Q_i &:= [x_{i-1}, x_i] && (i = 1, \dots, M), \\ m_i &:= \frac{x_i + x_{i-1}}{2} && (i = 1, \dots, M) \end{aligned}$$

be respectively the cell boundary points, the cells (as closed intervals) and the midpoints of the cells; see Figure 1. Let

$$h := |Q_i| = \frac{b-a}{M} > 0$$

be the cell size.

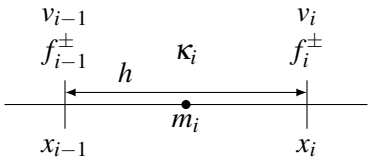

Figure 1: A cell Q_i.

Next we introduce the spatial discretization. We start from (1.2), which we derived from (P). To obtain the spatial discretization, we formally approximate the equations in (1.2) in terms of the average values of κ over Q_i given by

$$\kappa_i(t) := \frac{1}{h}\int_{x_{i-1}}^{x_i} \kappa(x,t)\,dx \qquad (i = 1, \dots, M).$$

In the following computations we remove the time variable. As done for (1.2) we split κ (and, similarly, κ_i) as $\kappa = \kappa^+ - \kappa^-$. Assuming that either $\operatorname{supp}\kappa^+$ or $\operatorname{supp}\kappa^-$ is disjoint with Q_i, we obtain by integrating both equations in (1.2) over Q_i that

$$\partial_t \kappa_i^+ = \frac{1}{h}\big(\kappa^+(x_{i-1})v(x_{i-1}) - \kappa^+(x_i)v(x_i)\big) \qquad \text{for all } 1 \leq i \leq M, \tag{3.1}$$

$$\partial_t \kappa_i^- = \frac{1}{h}\big(\kappa^-(x_{i-1})[-v(x_{i-1})] - \kappa^-(x_i)[-v(x_i)]\big) \qquad \text{for all } 1 \leq i \leq M. \tag{3.2}$$

Similar to (1.2), the only difference between the above two equations is the sign in front of the velocity v. Therefore, we focus on (3.1) in the following computations.

It is left to approximate the right-hand side of (3.1) by an expression which only depends on $\{\kappa_j\}_{j=1}^M$. First, we interpret $\kappa^+(x_j)v(x_j)$ as the flux at x_j. To encode the zero-flux boundary condition, we replace $\kappa^+(x_0)v(x_0)$ and $\kappa^+(x_M)v(x_M)$ by 0. Then, it is left to treat $\kappa^+(x_i)v(x_i)$ for

$1 \le i \le M-1$. With this aim, we approximate

$$\begin{aligned} v(x_i) &= \mathrm{PV}\int_a^b g(x_i-y)\kappa(y)dy \\ &= \sum_{j=1}^{M}\int_{Q_j} g(x_i-y)\kappa(y)dy \\ &\approx \sum_{j=1}^{M} g(x_i-m_j)\int_{Q_j}\kappa(y)dy \\ &= h\sum_{j=1}^{M} g(x_i-m_j)\kappa_j \\ &= \sum_{j=1}^{M}\frac{\kappa_j}{i-j+\frac{1}{2}} =: v_i. \end{aligned} \tag{3.3}$$

The second equality in (3.3) is formal, because $g(x_i-y)$ is not integrable on either Q_i or Q_{i+1}. We give a proper motivation for (3.3) in Section 3.4. Regarding $\kappa^+(x_i)$ for each $1 \le i \le M-1$, we approximate it by either κ_i^+ or κ_{i+1}^+ following the upwind direction, i.e.

$$\kappa^+(x_i) \approx \begin{cases} \kappa_i^+ & \text{if } v_i \ge 0, \\ \kappa_{i+1}^+ & \text{if } v_i < 0. \end{cases}$$

When we put this together, the flux is approximated for any $1 \le i \le M-1$ as

$$\kappa^+(x_i)v(x_i) \approx f_i^+ := \begin{cases} v_i\kappa_i^+ & \text{if } v_i \ge 0, \\ v_i\kappa_{i+1}^+ & \text{if } v_i < 0. \end{cases} \tag{3.4}$$

By setting $f_0^+ := f_M^+ := 0$, (3.4) holds for all $0 \le i \le M$. Finally, we obtain from (3.1) that

$$\partial_t \kappa_i^+ \approx \frac{1}{h}\left(f_{i-1}^+ - f_i^+\right) \qquad \text{for all } 1 \le i \le M. \tag{3.5}$$

Note that the right-hand side is explicit in terms of $\{\kappa_i\}_{i=1}^M$ as desired.

Next we apply a similar spatial discretization to (3.2). Since the only difference with (3.1) is that κ^- is driven by $-v$ as opposed to $+v$, only the expression for the flux changes. It changes into

$$f_i^- := \begin{cases} -v_i\kappa_i^+ & \text{if } v_i \le 0, \\ -v_i\kappa_{i+1}^- & \text{if } v_i > 0 \end{cases}$$

for any $1 \le i \le M-1$, and $f_0^- := f_M^- := 0$. Then, from (3.2) we obtain

$$\partial_t \kappa_i^- \approx \frac{1}{h}\left(f_{i-1}^- - f_i^-\right) \qquad \text{for all } 1 \le i \le M. \tag{3.6}$$

Finally, we discretize in time. We use the explicit Euler method with fixed time step $\tau > 0$. We add t back to the notation, and note that v_i and $f_i^\pm$ also depend on t. Let

$$t_k := \tau k \qquad (k = 0, \dots, K)$$

be the discrete time points, where $K := \lceil T/\tau \rceil$. We approximate

$$\partial_t \kappa_i^\pm(t_k) \approx \frac{\kappa_i^\pm(t_{k+1}) - \kappa_i^\pm(t_k)}{\tau}.$$

Then, setting

$$\kappa_i^{\pm,k} := \kappa_i^{\pm}(t_k)$$

and defining v_i^k and $f_i^{\pm,k}$ similarly, we obtain from (3.5) and (3.6) that

$$\kappa_i^{\pm,k+1} \approx \kappa_i^{\pm,k} + \frac{\tau}{h}(f_{i-1}^{\pm,k} - f_i^{\pm,k}). \tag{3.7}$$

Finally, we put $\kappa_i^{+,k+1}$ and $\kappa_i^{-,k+1}$ together to obtain κ_i^{k+1}. Note that $\{\kappa_i^{+,k+1}\}_{i=1}^M$ and $\{\kappa_i^{-,k+1}\}_{i=1}^M$ may overlap in the sense that there may exists an i for which $\kappa_i^{+,k+1}\kappa_i^{-,k+1} \neq 0$. Hence, they might *not* be the positive and negative part of some $\{\kappa_i^{k+1}\}_{i=1}^M$. To remove overlapping parts without changing the net charge, we simply set

$$\kappa_i^{k+1} := \kappa_i^{+,k+1} - \kappa_i^{-,k+1}. \tag{3.8}$$

This completes the motivation for the scheme below in Section 3.2.

However, the notation becomes inconsistent when iterating over k, because while $\kappa_i^{\pm,k}$ are the positive/negative part of κ_i^k, $\kappa_i^{\pm,k+1}$ need not be the positive/negative part of κ_i^{k+1}. Fortunately, by substituting (3.7) in (3.8), the use of $\kappa_i^{\pm,k+1}$ can be avoided. Indeed, this substitution yields

$$\kappa_i^{k+1} \approx \kappa_i^k + \frac{\tau}{h}(f_{i-1}^k - f_i^k) \qquad \text{for all } 1 \leq i \leq M,$$

where

$$f_j^k := f_j^{+,k} - f_j^{-,k} \qquad \text{for all } 0 \leq j \leq M.$$

3.2 Scheme

The scheme follows from the approximations in Section 3.1 by treating κ_i^k as an independent quantity and replacing all approximations by equalities. In more detail, for an initial condition $\{\kappa_i^0\}_{i=1}^M \in \mathbb{R}^M$, we iteratively compute $\{\kappa_i^{k+1}\}_{i=1}^M$ from $\{\kappa_i^k\}_{i=1}^M$ for $k = 0, \ldots, K-1$ as follows:

1. compute $v_i^k = \displaystyle\sum_{j=1}^{M} \frac{\kappa_j^k}{i-j+\frac{1}{2}}$ for $i = 1, \ldots, M-1$,
2. set $\kappa_i^{\pm,k}$ as the positive and negative part of κ_i^k for $i = 1, \ldots, M$,
3. for $i = 1, \ldots, M-1$ compute

$$f_i^{+,k} = \begin{cases} v_i^k \kappa_i^{+,k} & \text{if } v_i^k \geq 0 \\ v_i^k \kappa_{i+1}^{+,k} & \text{if } v_i^k < 0 \end{cases} \quad \text{and} \quad f_i^{-,k} = \begin{cases} -v_i^k \kappa_i^{-,k} & \text{if } v_i^k \leq 0 \\ -v_i^k \kappa_{i+1}^{-,k} & \text{if } v_i^k > 0, \end{cases}$$

4. set $f_0^k = f_M^k = 0$ and take $f_i^k := f_i^{+,k} - f_i^{-,k}$ for $i = 1, \ldots, M-1$,
5. compute $\kappa_i^{k+1} = \kappa_i^k + \frac{\tau}{h}(f_{i-1}^k - f_i^k)$ for $i = 1, \ldots, M$.

For convenience we further set $f_0^{\pm,k} = f_M^{\pm,k} = 0$ for all $0 \leq k \leq K$.

3.3 Properties and computational complexity

Let $a < b$, $M \in \mathbb{N}$, $T, \tau > 0$ and $\{\kappa_i^0\}_{i=1}^M$ be given, let h, K be as in Section 3.1 and let $v_i^k, f_i^{\pm,k}, f_i^k, \kappa_i^k$ be as defined by the scheme in Section 3.2. The computational complexity of the scheme is $O(M^2K) = O(h^{-2}\tau^{-1})$. Indeed, the scheme is iterated K times. At each iteration, Steps 2-5 take $O(M)$ many computations, but Step 1 requires $O(M^2)$ many computations.

Regarding the properties of the scheme, we show below in Proposition 3.1 that the discrete net charge given by

$$N_h^k := h\sum_{i=1}^{M} \kappa_i^k \qquad (k=0,\dots,K) \tag{3.9}$$

is unconditionally conserved. Moreover, in Proposition 3.3 we show that nonnegativity of $\{\kappa_i^k\}_{i=1}^M$ is conserved and that the total charge

$$B_h^k := h\sum_{i=1}^{M} |\kappa_i^k| \qquad (k=0,\dots,K) \tag{3.10}$$

is non-increasing in k for τ small enough with respect to h and B_h^0.

Proposition 3.1. *$N_h^k = N_h^0$ for all $0 \le k \le K$.*

Proof. Proposition 3.1 follows from induction by the following computation:

$$N_h^{k+1} = h\sum_{i=1}^{M} \kappa_i^{k+1} = h\sum_{i=1}^{M} \left(\kappa_i^k + \frac{\tau}{h}(f_{i-1}^k - f_i^k)\right) = N_h^k + \tau(f_0^k - f_M^k) = N_h^k. \tag{3.11}$$

□

Lemma 3.2. *For all $1 \le i \le M$ and all $0 \le k \le K$,*

$$f_{i-1}^{\pm,k} - f_i^{\pm,k} \ge -\frac{4}{h}\kappa_i^{\pm,k} B_h^k.$$

Proof. We prove the inequality with '$+$' in the superscript; the proof for when the superscript is '$-$' is analogous. For $c \in \mathbb{R}$ we set $[c]^+, [c]^- \ge 0$ as the positive and negative part. First, we assume that $2 \le i \le M-1$. By the definition of $f_j^{+,k}$,

$$f_{i-1}^{+,k} - f_i^{+,k} \ge -[v_{i-1}^k]^- \kappa_i^{+,k} - [v_i^k]^+ \kappa_i^{+,k},$$

where for $\ell \in \{i-1, i\}$

$$|v_\ell^k| = \left|\sum_{j=1}^{M} \frac{\kappa_j^k}{\ell - j + \frac{1}{2}}\right| \le 2\sum_{j=1}^{M} |\kappa_j^k| = \frac{2}{h} B_h^k. \tag{3.12}$$

Hence, Lemma 3.2 follows for $2 \le i \le M-1$. If instead $i \in \{1, M\}$, then the computation above simplifies since $f_0^{+,k} = f_M^{+,k} = 0$. □

Proposition 3.3. *If $\tau \le h^2/(4B_h^0)$, then the following hold:*

1. *$B_h^{k+1} \le B_h^k$ for all $k = 0,\dots,K-1$;*
2. *Let $k \in \{0,\dots,K-1\}$. If $\kappa_i^k \ge 0$ for all $1 \le i \le M$, then $\kappa_i^{k+1} \ge 0$ for all $1 \le i \le M$;*
3. *Let $k \in \{0,\dots,K-1\}$. If $\kappa_i^k \le 0$ for all $1 \le i \le M$, then $\kappa_i^{k+1} \le 0$ for all $1 \le i \le M$.*

Proof. We prove the first statement by induction over k. Suppose that $B_h^k \le B_h^{k-1} \le \dots \le B_h^0$ for some $k \in \{0,\dots,K-1\}$. Then,

$$\tau \le \frac{h^2}{4B_h^0} \le \frac{h^2}{4B_h^k}, \tag{3.13}$$

and by Lemma 3.2

$$\mu_i^{\pm,k} := \kappa_i^{\pm,k} + \frac{\tau}{h}(f_{i-1}^{\pm,k} - f_i^{\pm,k}) \ge \kappa_i^{\pm,k}\left(1 - \frac{4\tau}{h^2} B_h^k\right) \ge 0 \qquad (i=1,\dots,M). \tag{3.14}$$

Then, by a similar computation as in (3.11), we obtain the desired result from

$$B_h^{k+1} = h\sum_{i=1}^{M} |\kappa_i^{k+1}| = h\sum_{i=1}^{M} |\mu_i^{+,k} - \mu_i^{-,k}| \le h\sum_{i=1}^{M} (\mu_i^{+,k} + \mu_i^{-,k}) = B_h^k.$$

To prove the second statement, note that (3.13) holds and that $f_j^{-,k} = 0$ for all $0 \le j \le M$. Then,

$$\kappa_i^{k+1} = \kappa_i^{+,k} + \frac{\tau}{h}(f_{i-1}^{+,k} - f_i^{+,k}),$$

which, by repeating the computation in (3.14), is nonnegative for all $1 \le i \le M$. □

Remark 3.4. *The requirement in Proposition 3.3 that $\tau \le h^2/(4B_h^0) = O(h^2)$ is rather strict given that the stability condition for the finite volume method for the continuity equation with constant velocity is $\tau \le Ch = O(h)$. The additional factor h appears in the estimate in* (3.12)*, which is based on the worst case scenario in which κ_i^k is concentrated around the singularity of g. If we would have a uniform bound $|\kappa_i^k| \le C$ which holds for all $1 \le i \le M$ and all $0 \le k \le K$ (this bound turns out to hold for all simulations performed in Section 4), then the estimate in* (3.12) *can be sharpened to*

$$\begin{aligned} |v_\ell^k| &\le \sum_{j=1}^{M} \frac{|\kappa_j^k|}{|\ell - j + \frac{1}{2}|} \le \sum_{j=1}^{M} \frac{C}{|\ell - j + \frac{1}{2}|} \le 2C\Big(2 + \sum_{i=1}^{M-1} \frac{1}{i+\frac{1}{2}}\Big) \\ &\le 2C\Big(2 + \int_{\frac{1}{2}}^{M} \frac{1}{x}\,dx\Big) \le 2C\Big(2 + \log\frac{b-a}{h} + \log 2\Big) = O(|\log h|), \end{aligned}$$

and the required upper bound on τ in Proposition 3.3 would become of size $O(h|\log h|)$.

3.4 Proper motivation for v_i

Here we give a proper motivation for the formal computation in (3.3). We fix $i \in \{1,\dots,M-1\}$ and assume that $\kappa \in C([a,b])$ is differentiable at x_i. Because of the singularity in g, we have to consider the integrals over Q_i and Q_{i+1} together as a principal value integral, i.e.

$$\mathrm{PV}\int_{x_{i-1}}^{x_{i+1}} g(x_i - y)\kappa(y)dy = \lim_{\varepsilon\to 0}\left(\int_{x_{i-1}}^{x_i-\varepsilon} g(x_i-y)\kappa(y)dy + \int_{x_i+\varepsilon}^{x_{i+1}} g(x_i-y)\kappa(y)dy\right).$$

Using the oddness of g, we can rewrite the right-hand side as

$$\lim_{\varepsilon\to 0}\left(\int_{\varepsilon}^{h} 2zg(z)\frac{\kappa(x_i - z) - \kappa(x_i + z)}{2z}dy\right).$$

Then, in the integrand, $zg(z) \equiv 1$ and the fraction converges to $-\kappa'(x_i)$ as $z \to 0$. Hence, the limit $\varepsilon \to 0$ exists. By the midpoint rule for integration, we obtain that the limit is approximately equal to

$$2h\frac{\kappa(m_i) - \kappa(m_{i+1})}{h} \approx hg\Big(\frac{h}{2}\Big)\kappa_i + hg\Big(-\frac{h}{2}\Big)\kappa_{i+1}.$$

The two terms in the right-hand side are precisely the two terms in the sum in (3.3) corresponding to $j = i$ and $j = i+1$.

4 Simulations

In this section we examine the performance of the scheme for problem (P) in Section 3.2 by means of numerical simulations. We also examine the features of the numerical solution. In all simulations we take

$$\begin{aligned}
[a,b] &= [-3,3],\\
M &= 12\cdot 2^{\ell} \quad \text{for } \ell \in \{0,\dots,8\},\\
\tau &= \frac{1}{10M} = \frac{h}{60},\\
\kappa_i^0 &= \frac{1}{h}\int_{Q_i} \kappa^\circ(x)dx \quad \text{for } i \in \{1,\dots,M\},
\end{aligned}$$

where we consider three different choices for κ° in respectively Sections 4.1, 4.2 and 4.3. Note that by the choice of κ_i^0, we precisely capture the net charge (recall (2.2) and (3.9)) of κ°:

$$N_h^0 = h\sum_{i=1}^{M}\kappa_i^0 = \int_a^b \kappa^\circ(x)dx = N(0).$$

Recall from Proposition 3.1 that the scheme conserves the net charge. In Section 4.4 we summarize our observations and findings.

4.1 Self-similar solution

We start with the case in which κ° is a half-ellipse, such that the solution κ to (P) is explicitly given by a time translated version of the self-similar solution κ_* defined in (2.1) until the time T at which the support of $\kappa_*(\cdot,t)$ touches the endpoints of $[a,b]$. We take

$$\kappa^\circ(x) = \frac{8}{\pi}\sqrt{[\tfrac{1}{4}-x^2]_+},$$

which equals $\kappa_*(x,\frac{1}{16})$ with total charge $B(0)=N(0)=1$. Then,

$$\kappa(x,t) = \kappa_*\Big(x,t+\frac{1}{16}\Big) = \frac{1}{2\pi(t+\frac{1}{16})}\sqrt{[4(t+\tfrac{1}{16})-x^2]_+}.$$

Note that at $t=\frac{3}{16}$ and $t=\frac{15}{16}$ the support of $\kappa(\cdot,t)$ is respectively $[-1,1]$ and $[-2,2]$. Since $\kappa(x,t)\geq 0$, the scheme reduces to a standard application of the finite volume method. However, due to our simple discretization of the velocity in (3.3) it is not clear whether the discrete solution κ_i^k resembles $\kappa(x_i,t_k)$. Therefore, we first test our scheme for κ° above without any negative charge.

Figure 2 illustrates κ_i^k alongside $\kappa(x,t)$ at $t=0,\frac{3}{16},\frac{15}{16}$. Here and in what follows, at a given time point t, we take $k=\lceil t/\tau\rceil$ as the corresponding iteration number (note that $t\in(t_{k-1},t_k]$). It appears that the scheme is able to capture $\kappa(x,t)$ well without any speed up or lag in t. One noteworthy difference between κ_i^k and $\kappa(x,t)$ is that at the endpoints of the support of $\kappa(\cdot,t)$, where $\kappa(\cdot,t)$ sharply hits 0, κ_i^k regularizes the decay to 0. We observe that this regularization becomes smaller as M increases. For large values of M, the gray surface which represents κ_i^k resembles a blob with regular boundary; in the remainder (Figures 5 and 7) we will illustrate κ_i^k by this boundary as a line plot.

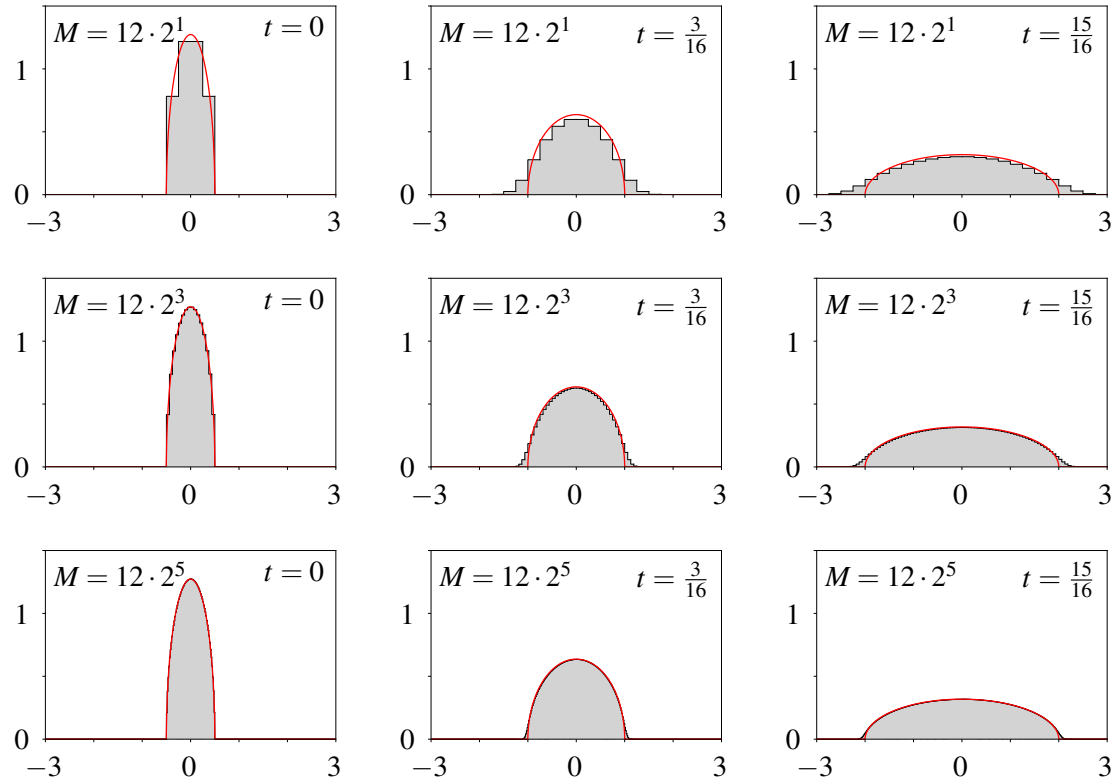

Figure 2: κ_i^k (gray) alongside $\kappa(x,t)$ (red) at $t = 0, \frac{3}{16}, \frac{15}{16}$ and for $M = 12 \cdot 2^\ell$ with $\ell = 1,3,5$.

To test and quantify the convergence of the scheme to (P), we define the relative error

$$\tilde{\varepsilon}_M(t) := \frac{1}{MB_h^k} \sum_{i=1}^{M} |\kappa_i^k(M) - \kappa(m_i,t)|, \tag{4.1}$$

which is based on the vector 1-norm. Recall that m_i is the midpoint of cell Q_i. We write $\kappa_i^k = \kappa_i^k(M)$ to emphasize the dependence on M. Since κ_i^k remains nonnegative, we obtain for the total charge B_h^k (i.e. h times the vector 1-norm of $\{\kappa_i^k\}_{i=1}^M$; recall (3.10)) that $B_h^k = N_h^k = N_h^0 = N(0) = 1$ for all $0 \le k \le K$.

Figure 3 suggests that the decay of $\tilde{\varepsilon}_M$ is close to first order in $\frac{1}{M}$. This is a surprisingly fast decay, because the standard finite volume method for the continuity equation with *constant* velocity has first order decay while the velocity in (P) is not constant and depends moreover on κ in a nonlocal and singular manner. Another interesting observation from Figure 3 is that $\tilde{\varepsilon}_M(t)$ seems to *decrease* in t. We think that this is due to the following. As time increases, the support of $\kappa(x,t)$ spreads out over more cells, and thus $\kappa(x,t)$ can be discretized more accurately over the cells (see the first row of three plots in Figure 2). However, that the scheme actually does this is surprising to us. It indicates that there is no artificial speed-up or lag in time.

The error in (4.1) is of limited practical use, because it requires the exact solution κ to be known. In preparation for testing our scheme with κ° for which we do not have an explicit expression, we define the relative error

$$\varepsilon_M(t) := \frac{1}{MB_h^k} \sum_{i=1}^{M} \left| \kappa_i^k(M) - \frac{\kappa_{2i-1}^k(2M) + \kappa_{2i}^k(2M)}{2} \right|.$$

This error compares the discrete solution $\kappa_i^k(M)$ to that on a grid which is twice as fine (i.e. to

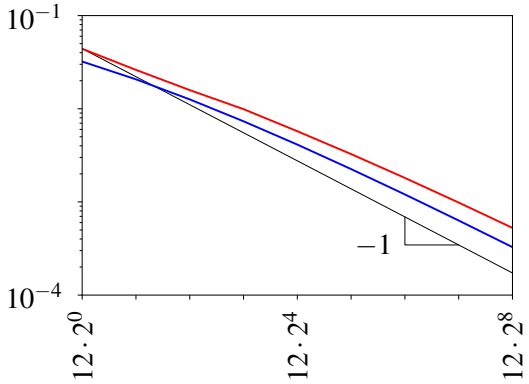

Figure 3: The error $\tilde{\varepsilon}_M(t)$ as a function of M for κ° as the half ellipse and for $t = \frac{3}{16}$ (red) and $t = \frac{15}{16}$ (blue).

$\kappa_i^k(2M)$). The number of fine cells, i.e. $2M$, is chosen such that each cell on the coarse grid covers precisely two neighboring cells on the fine grid.

Figure 4 shows that $\varepsilon_M(t)$ is qualitatively similar to $\tilde{\varepsilon}_M(t)$. In particular, the decay with respect to $\frac{1}{M}$ seems to be roughly of first order, which implies on itself that the decay of $\tilde{\varepsilon}_M(t)$ is roughly of first order too. This motivates us to work with $\varepsilon_M(t)$ in all simulations which follow.

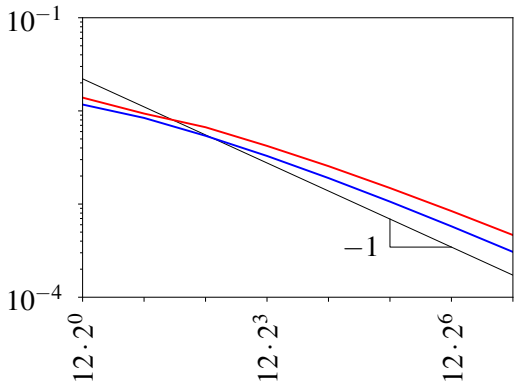

Figure 4: Similar as Figure 3, but now for the error $\varepsilon_M(t)$.

4.2 Two asymmetric positive blocks

In Section 4.1 we demonstrated that the scheme performs well for the self-similar solution. Here we investigate its performance for a more generic solution. We still limit κ° to be non-negative in order to discover the effect of the simple approximation for the velocity in (3.3).

More precisely, we investigate the evolution of two positive blobs of different size. With this aim, we take

$$\kappa^\circ(x) = \begin{cases} 1 & \text{if } x \in [-1, \frac{1}{2}] \cup [0,1] \\ 0 & \text{otherwise;} \end{cases} \tag{4.2}$$

see Figure 5. First we examine κ_i^k for $M = 12\cdot 2^8$ to study features of the solution κ to (P). From Figure 5 we make three interesting observations:

- Shortly before the two blobs aggregate (at $t = 0.13$), the influence of one blob on the profile of the other is hardly visible. In particular, close to the point of contact the blobs do not seem to anticipate the aggregation. The effect of the nonlocal (repelling) force of the small blob exerted on the big blob is visible from the small shift of the big blob to the right.
- Shortly after the two blobs have aggregated (at $t = 0.17$), the kink in the graph of κ_i^k close to where the two blobs met is still profoundly visible. Therefore, the smoothing effect of (P) seems to be weak.
- At $t = 1$, which is long after the aggregration of the blobs but before κ_i^k hits either of the endpoints of $[a,b]$, the graph of κ_i^k starts to resemble the self-similar solution. This is in line with the stability result established in [BKM10].

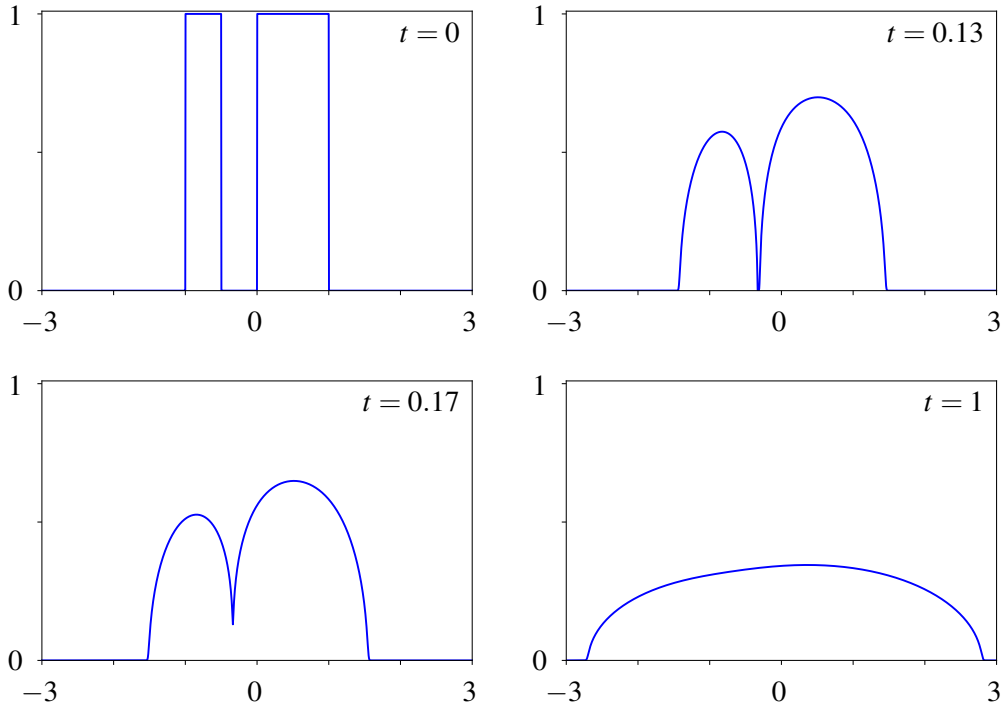

Figure 5: κ_i^k (blue) for $M = 12 \cdot 2^8$ and κ° as in (4.2) at several time points.

Next we examine the convergence of κ_i^k as M gets large. Figure 6 suggests that the error $\varepsilon_M(t)$ has again roughly a first-order decay with respect to $\frac{1}{M}$. Hence, the good performance of the scheme extends beyond the self-similar solution. We also observe that $\varepsilon_M(t)$ seems to be decreasing in t when M is large enough.

We remark that while the decay of $\varepsilon_M(t)$ in M suggests convergence of the scheme, it does not necessarily follow that the limit is given by the solution κ of (P). However, we have validated that κ_i^k is close to the numerical solution of the particle system in (1.3) (see e.g. [Pra20] for an accurate numerical scheme), and [vMPP22] guarantees that the particle system converges to (P).

4.3 Two asymmetric blocks of opposite charge

Finally, we consider a choice for κ° which takes both signs such that we can test the part of the scheme where it deviates from the finite volume method. To compare with the setting in Section

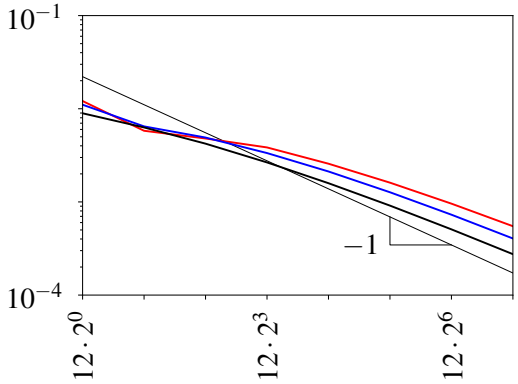

Figure 6: The error $\varepsilon_M(t)$ as a function of M for κ° given by the two positive blocks and for $t = 0.1$ (red), $t = 0.2$ (blue) and $t = 0.5$ (black).

4.2 (see (4.2)), we take

$$\kappa^\circ(x) = \begin{cases} -1 & \text{if } x \in [-1, \frac{1}{2}] \\ 1 & \text{if } x \in [0,1] \\ 0 & \text{otherwise;} \end{cases} \tag{4.3}$$

see Figure 7. As for the previous case, we examine κ_i^k for $M = 12 \cdot 2^8$ to study the features of the solution κ to (P). From Figures 5 and 7 we make three interesting observations:

- At $t = 0.04$, shortly before the two blobs collide, it appears again that the shapes of the blobs are hardly influenced by the presence of the other blob, and that there is no visible anticipation of the shape prior to collision. In comparison to Figure 5, the blobs have slightly moved *towards* each other, and the collision happens much earlier.
- At $t = 0.2$, well after the blobs have collided, it is clear from the size of the smaller blob that a certain amount of charge has been neutralized. We also observe that the graph of κ_i^k is steep around the contact point (steeper than on neighborhoods around the two endpoints of its support). We have no conjecture about the (asymptotic) shape of κ_i^k around the contact point.
- At $t = 1$ most of the charge of the small blob has been neutralized, and the support of κ_i^k is not far from the endpoint b. Both blobs seem to expand (i.e. they get closer to their corresponding endpoints a or b) despite the attractive force exerted by the other blob. The contact point seems to move to the left. We also note that the positive blob may seem to have moved to the *right* despite the attractive force exerted by the negative blob. Our explanation for this is as follows: the figure only shows the *remaining* positive charge, whereas all the neutralized positive charge is piled up along the area swept over by the contact point.

Next we examine the convergence of κ_i^k as M gets large. Figure 8 suggests that the error $\varepsilon_M(t)$ has again roughly a first-order decay with respect to $\frac{1}{M}$, but the evidence is less strong than in the previous case (see Figure 6). Indeed, larger values of M are needed to observe convergence, and for $t = 0.02$ (prior to collision) the available data show a lower rate of convergence. Nevertheless, the scheme seems to perform well also for initial conditions with both positive and negative charge distributions. In addition, we observe again that (for M large enough) $\varepsilon_M(t)$ is decreasing in time. Finally, we have again validated that κ_i^k is close to the solution κ of (P) by comparing it to the solution of the particle system in (1.3).

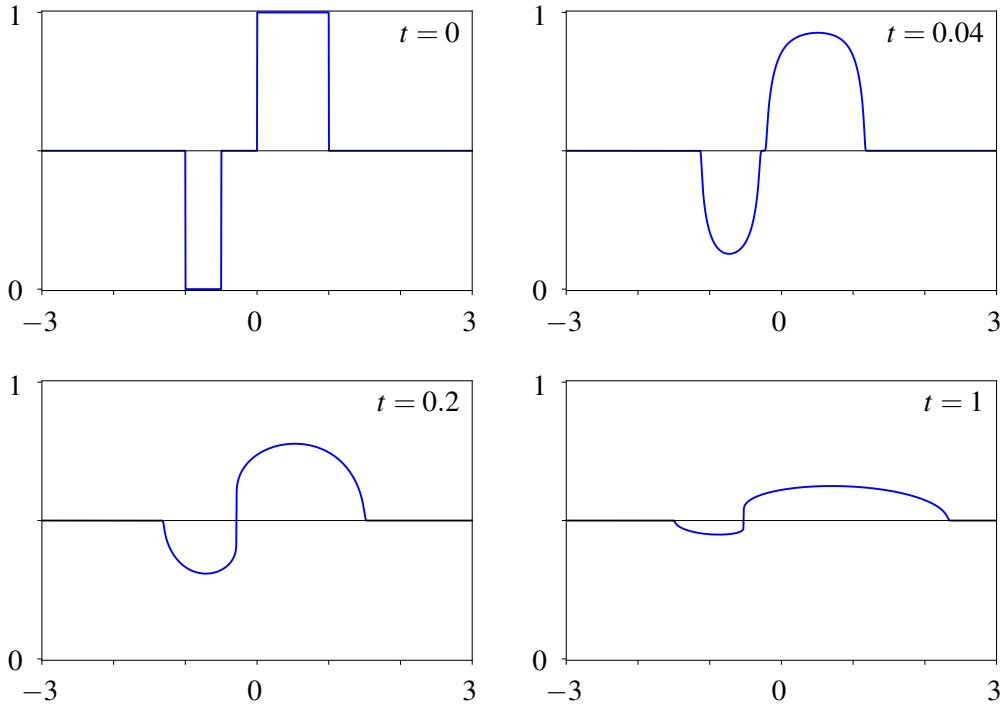

Figure 7: κ_i^k (blue) for $M = 12 \cdot 2^8$ and κ° as in (4.3) at several time points.

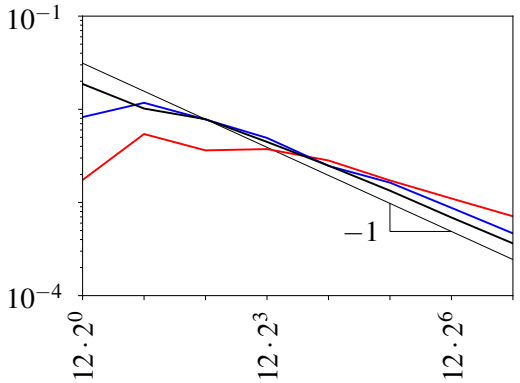

Figure 8: Similar to Figure 6, but now for κ° given by the two blocks of opposite charge and for $t = 0.02$ (red), $t = 0.1$ (blue) and $t = 0.5$ (black).

4.4 Synopsis of the observations

In Sections 4.1, 4.2 and 4.3 we have tested the accuracy of the scheme and observed features of the numerical solution. Here, we focus on the common observations, and expect that they apply to any initial condition.

The accuracy of the scheme seems to be close to $O(\tau + h)$. This is surprisingly good, given the simplicity of the approximation of the nonlocal and singular flow field v (see (3.3)). As a consequence of this accuracy, the numerical solution converges. We observed that the limit appears to be indeed the solution κ to problem (P).

We also observed that the relative error *decreases* in time, which came as a surprise to us. This shows that there is no artificial speed up or lag induced by the scheme. We note that this

observation is based only on three time points. In fact, since there is no error at $t = 0$, there must be a short initialization period during which the error increases. Nonetheless, the decrease in error sets in long before the solution starts to resemble the self-similar solution.

The problem (P) tends to regularize $\kappa(\cdot,t)$ as t increases, but only for density values away from 0. At points where $\kappa(\cdot,t)$ hits 0, the derivative seems to blow up. This blow-up is even stronger at points where $\kappa(\cdot,t)$ changes sign.

As for the long-time behavior of (P), there appear to be two competing effects: the spreading out of density blobs and the attractive force between blobs of opposite charge. It would be interesting to find out which of the two effects will be dominant, i.e. whether $\lim_{t\to\infty} B(t)$ (recall (2.3)) equals 0 or not. However, our discretization in both time and space is not suited to address this question numerically.

5 Conclusion

For the mathematically rather complicated problem (P) which describes the evolution of the electric charge density κ, we have developed a simple numerical scheme (see Section 3.2). The scheme is not restricted to $g(x) = \frac{1}{x}$, and can easily be extended to other interaction forces g as long as g is odd and $|xg(x)|$ is integrable around $x = 0$. The numerically tested performance of the scheme is very good in the sense that its accuracy is close to the best accuracy one can expect from an upwind scheme with explicit Euler time integrator. Also, the scheme appears to have no artificial speed up or lag in time (in fact, the relative error tends to decrease in time for all tested scenarios), and conserves the expected properties of κ.

We wish to mention four directions for future research:

1. It would be interesting to see whether the computational cost can be reduced (up to almost one order in M) without giving up too much on accuracy. The idea is that in Step 1 of the scheme (in the computation of v_i^k) the values of κ_j^k with j far from i get a smaller weight compared to those for j close to i. Thus, by using a hierarchy of coarser cells (multi-grid), several adjacent values κ_j^k can be clogged together to reduce the size of the sum in Step 1 without losing too much accuracy.
2. (P) should be discretized on $\mathbb{R}$ instead of a bounded interval $[a,b]$. This becomes relevant when studying the long-time behavior. For this, both the spatial and temporal grid need to be carefully designed.
3. The numerically observed good performance of the scheme further motivates to rigorously establish accuracy of the scheme. However, we think that this is very challenging due to the singular nature of the PDE (P) and the lack of regularity of its solution (see e.g. Figure 7).
4. The extension of the scheme to two spatial dimensions is much desired. Indeed, while the counterpart of the PDE in (P) in two dimensions can formally be written as

$$\frac{\partial \kappa}{\partial t} = -\operatorname{div}\left(|\kappa|\,(g_2 * \kappa)\right), \qquad g_2(x) := \frac{x}{|x|^2},$$

no well-posed solution concept is available for either this equation (an attempt was made in [AMS11]) or for the corresponding particle system in two dimensions. Yet, since our scheme is mainly based on the finite volume method, it is not difficult to extend it to two dimensions. It remains to investigate the performance of the scheme in two dimensions.

Acknowledgements

PvM was supported by JSPS KAKENHI Grant Number JP20K14358.

References

[AMS11] L. Ambrosio, E. Mainini, and S. Serfaty. Gradient flow of the Chapman–Rubinstein–Schatzman model for signed vortices. In *Annales de l'Institut Henri Poincare (C) Non Linear Analysis*, volume 28, pages 217–246. Elsevier, 2011.

[BKM10] P. Biler, G. Karch, and R. Monneau. Nonlinear diffusion of dislocation density and self-similar solutions. *Communications in Mathematical Physics*, 294(1):145–168, 2010.

[IMR08] C. Imbert, R. Monneau, and E. Rouy. Homogenization of first order equations with (u/ε)-periodic Hamiltonians Part II: Application to dislocations dynamics. *Communications in Partial Differential Equations*, 33(3):479–516, 2008.

[Pra20] H. Prayogi. Explicit variable time step solver for particle dynamics in 1d with an annihilation rule. Master's thesis, Kanazawa University, 2020.

[vMPP22] P. van Meurs, M. A. Peletier, and N. Požár. Discrete-to-continuum convergence of charged particles in 1D with annihilation. *Archive for Rational Mechanics and Analysis*, 246(1):241–297, 2022.